Proceedings of ASME Turbo Expo 2011
GT2011
June 6-10, 2011, Vancouver, British Columbia, Canada

GT2011-45668

THE EFFECT OF THE OPERATING CONDITIONS OF THE LAST TURBINE STAGE ON THE PERFORMANCE OF AN AXIAL EXHAUST DIFFUSER

Victor Opilat, Joerg R. Seume
Institute of Turbomachinery and Fluid Dynamics
Leibniz Universität Hannover
Appelstr. 9, 30167 Hannover, Germany
E-Mail: Opilat@tfd.uni-hannover.de, Seume@tfd.uni-hannover.de

ABSTRACT

The exhaust diffusers studied in this paper are installed behind the last turbine stage of gas turbines, including those used in combined cycle power plants. For the design of efficient diffusers, the effects caused by the last turbine stage need to be taken into account.

In the present paper, results are presented to estimate the performance of a diffuser operating under a variation of multiple modelling parameters: tip leakage flow, the swirl, and the rotating blade wakes. To provide a better understanding of the flow parameters, a test facility with a turbine stage simulator is used to model these flow effects and an optical endoscopic planar measurement technique based upon Particle Image Velocimetry (PIV) is applied.

The pressure recovery is estimated for various turbine conditions using a variety of relevant parameters. Within a range of conditions, a PIV study is performed to try to understand the typical flow phenomena which influence the performance of axial diffusers.

The rise of turbulent energy in the inlet flow positively affects the diffuser performance. A small positive swirl angle in the inlet flow (behind the rotating bladed wheel in experiments) has a stabilizing effect on the diffuser. The tip leakage flow from the last turbine stage can also positively affect the pressure recovery in the diffuser.

NOMENCLATURE

A	[m²]	cross section
n	[rpm]	rotational speed of the bladed wheel
$\dot{m}$	[kg/s]	mass flow
r_{Euler}	[m]	Eulerian radius
u	[m/s]	circumferential velocity of bladed wheel
ρ	[kg/m^3]	density
c	[m/s]	velocity
X, Y	[mm]	coordinates in the PIV measured region
Ma	[-]	Mach number at the diffuser inlet, at 50% channel height
c_p	[-]	pressure recovery coefficient
φ	[-]	flow coefficient
ω_z	[1/s]	the out-of-XY-plane vorticity
$\upsilon = \frac{R_i}{R_{out}}$	[-]	R_i is the inner radius, R_{out} is the outer radius
$L_{ann}* = \frac{L}{h}$, $L_{con}* = \frac{L}{R}$		dimensionless length of diffuser, using
L	[mm]	length of diffuser
h	[mm]	channel height (for the annular diffuser)
R	[mm]	outer radius of the channel (for the conical diffuser)

Subscripts

ax	axial
r	radial
tg	circumferential
1, (2)	inlet (outlet) of the annular diffuser
tot	total

INTRODUCTION

Exhaust diffusers are installed behind the last turbine stage of stationary gas turbines, including gas turbines used in combined power plants upstream of the HRSG (heat recovery steam generator). The purpose of an exhaust diffuser is to guide the turbine exhaust flow to the heat exchanger in order to recover thermal energy from it. Due to the flow passing through the diffuser, the pressure in the flow increases and the velocity decreases. A part of the kinetic energy of the exhaust

flow is transformed into static pressure. The diffuser thus increases the enthalpy change in the turbine and makes the combined cycle plant work more efficiently.

Geometrically, diffusers are axis-symmetric channels, in which the cross-sectional area increases with its length. Diffusers consist of an annular and a conical part. The hub in the annular part is needed to accommodate the rear bearing of the turbine rotor and is supported with struts connecting it to the casing. The conical part connects the annular part with the downstream units. The performance of diffusers is traditionally measured with the pressure recovery coefficient c_p showing which portion of the exhaust energy was transformed into static pressure.

Lechner and Seume [1] explain the working principle of a diffuser and other exhaust system parts of a gas turbine and provide examples of its implementation. It is stated that still no optimal technology exists for the diffuser component, and that manufacturers still use conventional concepts. The option of hub extension for reduction of losses at the annular diffuser end used by GE and Siemens (formerly Westinghouse) is explicitly not considered to be the best choice compared with the abrupt ending of the hub. The problem of flow disturbance from the downstream installed components is mentioned.

The Siemens H class turbine SGT5-8000H possesses an axial exhaust diffuser, as described by Fischer [2]. GE employs axial diffusers in their F-class heavy duty gas turbines. In the B- and E-class turbines, radial diffusers are used, as described by Balevic et al. [3].

Improving diffuser performance by optimizing its design is the main goal. Design optimisation of a diffuser requires consideration of the turbine working conditions as shown by Kruse and Quest [4]. When the load at the gas turbine is changed, the mass flow changes and the turbine exhaust flow pattern is changed. The incoming flow is swirled. The flow in the diffuser is always unsteady due to the operation of the upstream turbine and also can have fluctuations because of the downstream units (e.g. heat exchanger) and the unwanted boundary layer separation from the diffuser walls.

A well-known tool for diffuser design is the work of Sovran and Clomp [5], which provides performance charts for a range of diffuser geometries but with no consideration of the turbine. The goal of diffuser research since then has been the search for an alternative to the performance charts of Sovran and Clomp for enabling better design of diffusers, which should consider unsteady effects and secondary flows in diffusers.

Numerical investigation of the diffusers has progressed in the last years. An extensive numerical investigation of the impact of blade wakes was provided by Kluß et al. [6]. This research with the commercial solver ANSYS CFX-10.0 has shown that only an unsteady approach with the shear stress transport turbulence model is capable of predicting the stabilizing effect of the rotating wheel to the diffuser flow. It was suggested that the mixing effect of wakes and secondary flow pattern is responsible for the flow reattachment. However the calculation time for the unsteady approach is significant (up to a few weeks computer time). The CFD calculation results require validation with cutting-edge experimental data.

A common approach in the experimental research on diffusers as well as on the other turbomachinery units is the application of the newest measurement techniques. Extensive experimental research was carried out by Fleige et al. [7] and Sieker and Seume [8]. Pneumatic measuring of static pressures on the hub and casing inner surfaces in the diffuser as well as measuring of static and total pressures using more-hole probes for estimation of the pressure recovery coefficient and the loss coefficients can be supplemented for a better understanding of the flow pattern. Two examples of supplementation are the LDA velocity measurements as performed by Sieker and the planar optical measurements of velocity. Sieker investigated the pressure recovery in diffusers using a rotating spoke wheel and a NACA-bladed wheel in order to simulate turbine rotor wakes. It was shown that the flow field as well as the pressure recovery in the annular diffuser strongly depend on the spoke wheel operating conditions.

Chernikov [9, 10] studied diffuser performance under changes in load on an air supplied turbine stage. A precise scale model of the last turbine stage was used to generate the inflow into the diffuser. Pneumatic 5-hole probes and thermoelectric elements were used for measuring pressure and temperature, respectively. Chernikov found a significant influence of the turbine operating mode on the diffuser characteristics and considered the interaction of the tip leakage flow with the secondary flows to explain the phenomena. The highest pressure recovery was found for moderate positive swirl in the main flow. Chernikov suggested that the interaction of the main flow vector, the leakage flow vector and the secondary flows in the close-to-shroud part are responsible for the flow stabilisation. The emerging vortex chain is energised and works downstream in the diffuser. The highest pressure recovery was found for the operating points where the inflow has high kinetic energy and swirl while the flow at the hub is almost non-swirled.

The similarity of geometric parameters of the test rig used in the current research and those of Chernikov (see Annex) allows comparison though it is limited by the technical boundary conditions (geometry of the test rigs, limits of modelling at the test rig). The diffuser test rig in the current research is a geometrically scaled model of a real turbine exhaust diffuser for which nearly all flow parameters can be easily modified. By contrast, the diffuser test rig of Chernikov is closer to real turbine exhaust diffuser conditions and possesses a scaled model of turbine stage and two rows of guide vanes, in which parameters cannot be easily modified. A dimensionless comparison of results confirms the relevance of the dimensionless parameters and validates the results.

Further, the endoscopic Particle Image Velocimetry (PIV) method is applied in this research in combination with pneumatic measurement techniques for investigation of the

diffuser flow conditions. While being in development for 25 years, the PIV has been used in turbomachinery tests for just several years. The work of Alhaj and Seume [11], for example, showed a successful implementation of the PIV to a linear turbine blade cascade. A very comprehensive study of velocity fields using PIV and laser vibrometry behind a linear turbine cascade was performed by Woisetschlaeger et al. [12]. That study provided information about the flow, not only in terms of velocity fields and derivative variables, but also the frequency of density fluctuations in the flow. The current PIV approach stands out due to the implementation of a "rotating" test rig (though there have been tests on rotating machines described by Woisetschlaeger and Göttlich [13]) and use of endoscopes for both laser and camera where there is no need for windows matched to the test rig's surfaces.

EXPERIMENTAL FACILITY: DIFFUSER TEST RIG

The diffuser test rig at the Institute of Turbomachinery and Fluid-Dynamics, which was built up by Fleige, is a 1:10 scaled model of a gas turbine exhaust diffuser and is shown in Fig. 1. Different set-ups allow for easy varying of relevant flow parameters and for studying their impacts independently. The Mach number at the inlet is at maximum 0.16 and can be adjusted continuously. Mass flow is provided by a 37 kW fan. The test rig consists of an annular replaceable diffuser (a) with opening angles of 10°, 15°, or 20° and a following conical section (b) with an opening angle of 5°.

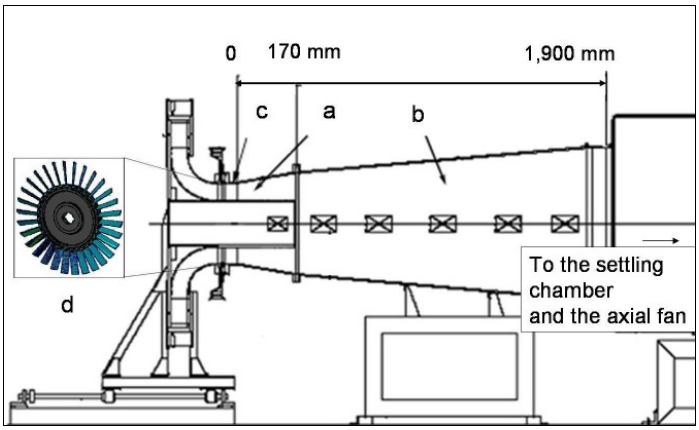

Figure 1: Test facility – a: annular diffuser; b: conical diffuser; c: tip leakage flow; d: bladed wheel

Tip leakage flow (c) can be brought into the flow in the annular diffuser inlet by a ca. 1.5 mm annular gap. Uniform flow is provided by four circumferential, uniformly-distributed corrugated tubes (see Fig. 2). Tip leakage flow is provided by an additional 5 kW centrifugal fan with adjustable frequency. In order to vary the swirl in the leakage flow in a range of ±25°, 30 sheet-metal swirl vanes are installed in the tip leakage flow set-up. The circumferential component in the leakage flow is adjusted by bending these vanes. Sieker and Seume [8] implemented a rotating spoke wheel in the inlet of the annular diffuser which simulates the flow conditions comming from the last turbine stage. Its rotational speed is variable up to 3,000 rpm and is provided by a 4 kW electric motor with a frequency converter. For the results presented in this paper, a symmetrical NACA-0020 wheel with 30 bladed spokes is used (d). The reasons for not using typical gas turbine blading in the rotor at this test rig are given by Sieker and Seume [8], i.e. the present bladed rotor is not a turbine stage but aims at generating a wake of eddy size and direction typical of turbine blade wakes. In absence of one or several upstream turbine stages, this was found to be best achieved by NACA blading. The design conditions for the bladed rotor are at a rotational speed of 2,500 rpm and a mass flow of 5.5 kg/s for the non-swirling flow.

INSTRUMENTATION

Three-hole pneumatic probes are used to measure total and static pressure distributions and the swirl angle in the inlet and outlet of the annular diffuser. Therefore the axial and the circumferential velocity components can be defined. In Fig. 2, traversing devices for the pressure probes can be found in the upper part of the ring diffuser in its inlet and outlet. For measuring the static pressure, 128 taps are installed along the annular and the conical diffuser and connected with an automated Pressure Systems Net Scanner. In the annular diffuser, the taps are located on the shroud and on the hub. The conical diffuser has taps on the shroud and on a narrow tube located along its centre line for providing the pressure channels.

The endoscopic PIV measurement technique is applied for the diffuser test rig. The principle of PIV is to visualise the flow using two pulsed lasers. The laser beams are guided from the laser head through optics which transform them into thin laser sheets which illuminate a measuring plane. The flow is seeded with light-weight, light-reflecting particles. The distribution of the illuminated particles in the two laser pulses is recorded by a digital camera with respect to the measurement time. As the time distance between the two laser pulses is known, the images can be correlated applying software generating velocity fields.

A setup for endoscopic and two-dimensional PIV is shown in Fig. 2. The laser endoscope is mounted on adjustable panels. The CCD Camera is mounted on a remote-controlled traverse, which allows endoscope positioning with an accuracy of 0.5 mm. Vegetable oil particles, which are brought into the flow upstream of the swirl generator by a perforated tube to ensure a homogeneous distribution, are used for seeding. The average size of the particles is 7 µm. Two Nd:YAG-Lasers, which operate in a pulsed mode, generate light with a wavelength of 532 nm and a pulse energy of 200 mJ per laser head.

The synchronizer coordinates the lasers and the camera with respect to a trigger signal. The trigger defines the time of flow illumination. Working with the internal trigger, the repetition rate of the PIV measurement was constant at 10 Hz. To

investigate the unsteady wakes behind particular blades, an external trigger is used, providing the measurement in delay mode with respect to the rotor position. The pulse distance in the tests is between 7 and 20 µs, what corresponds to a particle displacement of about 0.3 mm for a 50 m/s flow velocity. The laser light reflection from the NACA-blades and the hub surface was reduced by painting them with black colour. For estimation of the turbulence level, values of rms velocities are used. The averaged velocity fields and the deviations are calculated using statistical approaches in the evaluation software.

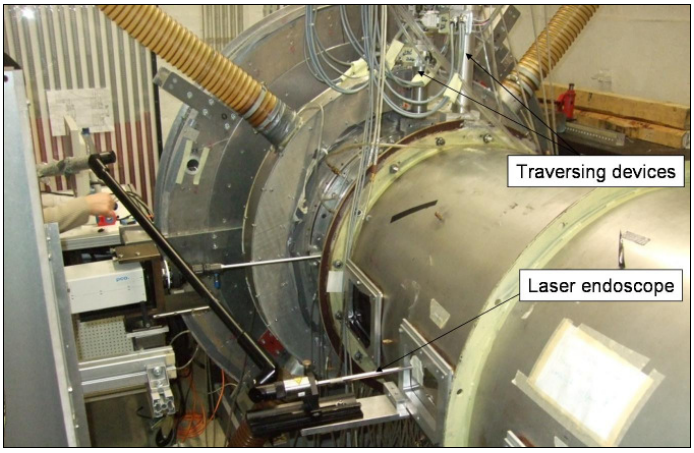

Figure 2: The setup for endoscopic PIV, view from diffuser

The PIV configuration applied to study the flow field in the axial and circumferential direction is shown in Fig. 3. A 70x100 mm section of the diffuser channel located immediately behind the bladed wheel is illuminated by the laser. Due to the opening angle of the light section and for maximizing the measurement region, the distance between the laser endoscope and the camera endoscope position was chosen to be 100 mm. The distance between the measurement plane and the camera endoscope is 50 mm, what results in high-quality correlations for a measuring section of 70x100 mm.

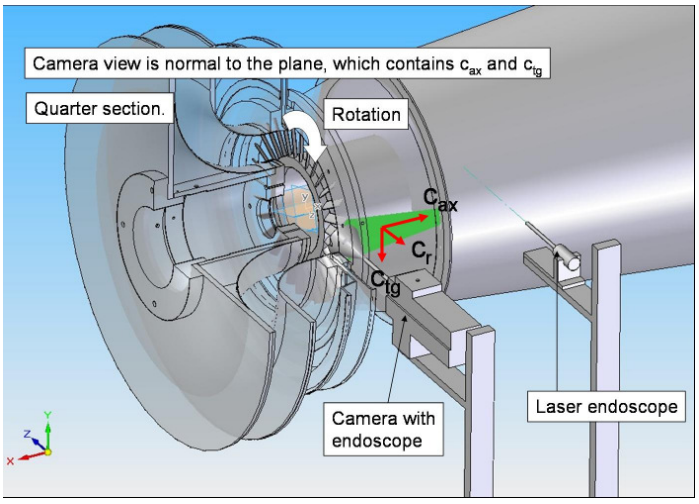

Figure 3: PIV set-up (the rotor carrying blades not shown)

TEST PROGRAM AND PARAMETERS

The inlet swirl is measured in negative and positive direction referring to the turbine operating conditions at partial load and over load, respectively. The 0° swirl refers to the diffuser design point. Each operating point can be described dimensionlessly using the flow parameter:

$$\varphi = \frac{\overline{c_{ax}}}{u_{Euler}} = \frac{\overline{\frac{\dot{m}}{\rho \cdot A}}}{2 \cdot \pi \cdot n \cdot r_{Euler} \cdot \frac{1}{60}} \qquad [1]$$

which is defined as the ratio between the mean axial velocity at the inlet with respect to the circumferential velocity using the Eulerian radius. Mass flow is calculated by averaging the radial distribution of the axial velocity over the channel height. At the inlet of the annular diffuser, the radial distribution of the total and static pressure as well as the swirl angle is measured using three-hole pneumatic probes. The pressure recovery coefficient is defined as

$$c_p = \frac{\overline{p_2} - \overline{p_1}}{\overline{p_{tot,1}} - \overline{p_1}} \qquad [2]$$

where $(p_2\text{-}p_1)$ is the rise of static pressure in the diffuser and $(p_{tot,1}\text{-}p_1)$ is the dynamic pressure at the inlet of the diffuser.
The flow vorticity used for flow pattern analysis is defined as

$$\omega_z = \left(\frac{\partial c_{tg}}{\partial x} - \frac{\partial c_{ax}}{\partial y}\right) \qquad [3]$$

To investigate the performance of the diffuser, experimental tests have been carried out for a diffuser consisting of a 15° annular part and a 5° conical part, with the NACA-bladed wheel as a turbine simulator, varying the mass flow (and therefore Mach number) and the swirl angle (and thus the flow coefficient). Table no. 1 shows the studied operating points.
For calculation of the turbulence intensity, the following correlations are applied as by PivTEC [14]:

Mean value $$\bar{x} = \frac{1}{N}\sum_{i=1}^{N} x_i \qquad [4]$$

Variance $$\sigma_x^2 = \frac{N\sum_{i=1}^{N} x_i^2 - \left(\sum_{i=1}^{N} x_i\right)^2}{N(N-1)} \qquad [5]$$

Standard velocity deviation, c', is defined as the square root of the variance. To analyze turbulent characteristics, the mean velocity components, $(\overline{c_{ax}}, \overline{c_{tg}})$ and the rms velocities (c'_{ax}, c'_{tg}), are used. The turbulent kinetic energy is defined as

$$k_{kin,turb,3D} = \frac{1}{2}\left(\overline{c'^2_{ax}} + \overline{c'^2_{tg}} + \overline{c'^2_{r}}\right) \qquad [6]$$

Table 1: Test parameters

Name	n, rpm	swirl angle main flow	Flow coefficient φ	c_p
15° annular + 5°conical diffuser + NACA-profiled rotor				
Ma=0.08 ($\dot{m} \approx 4$ kg/s)				
V121	2,100	-10°	0.65	0.61
V122	1,902	-5°	0.74	0.65
V123	1,758	0°	0.79	0.69
V124	1,590	5°	0.90	0.69
V125	1,498	10°	0.97	0.56
Ma=0.1 ($\dot{m} \approx 5$ kg/s)				
V102	2,436	-5°	0.72	0.63
V103	2,322	0°	0.76	0.65
V104	1,998	5°	0.88	0.73
V105	1,806	10°	0.99	0.68
V106	1,668	15°	1.06	0.62
Ma=0.1 ($\dot{m} \approx 5$ kg/s, $\dot{m}_{leakage} \approx 0.1$ kg/s) leakage swirl angle -20°				
V240	2,940	-15°	0.54	0.72
V241	2,724	-10°	0.59	0.78
V242	2,496	-5°	0.66	0.80
V243	2,286	0°	0.74	0.81
V244	2,052	5°	0.83	0.81
V245	1,818	10°	0.97	0.77
V246	1,608	15°	1.09	0.77
Ma=0.12 ($\dot{m} \approx 6$ kg/s)				
V161	3,000	-10°	0.66	0.51
V162	2,874	-5°	0.73	0.65
V163	2,604	0°	0.82	0.71
V164	2,346	5°	0.91	0.71
V165	2,136	10°	1.01	0.69
Ma=0.12 ($\dot{m} \approx 6$ kg/s, $\dot{m}_{leak.} \approx 0.14$ kg/s) leakage swirl angle -20°				
V262	3,000	-5°	0.66	0.81
V263	2,736	0°	0.74	0.81
V264	2,454	5°	0.84	0.82
V265	2,112	10°	0.99	0.79
Ma=0.14 ($\dot{m} \approx 6.5$ kg/s)				
V172	3,000	-5°	0.72	0.58
V173	2,816	0°	0.81	0.70
V174	2,546	5°	0.90	0.72

As the two-dimensional PIV is applied, the radial component can not be measured simultaneously with the axial and circumferential component. Therefore the radial component is considered constant and the following formula is used:

$$k_{kin,turb,2D} = \frac{3}{4}(\overline{c'_{ax}}^{\,2} + \overline{c'_{tg}}^{\,2}) \qquad [7]$$

The choice of the mass flow rate and the swirl in the leakage flow was set using the approach given by Fleige [7]. In the tests with swirled tip leakage flow, the velocity ratio between the leakage flow and the main flow was the highest at approximately 1.2. The direction of swirl in the leakage flow is adjusted using the relation:

$$\alpha_{leakage} \approx 0.25 \cdot \alpha_{main\_flow} - 19° \qquad [8]$$

Unlike the investigations of Fleige, a shorter diffuser (with 15° annular part) and the bladed wheel are used.

RESULTS OF EXPERIMENTAL INVESTIGATION

INFLUENCE OF THE SWIRL (AND TURBULENCE) ON THE PERFORMANCE OF THE DIFFUSER

The swirl used as a describing parameter is produced by the bladed wheel and therefore the influence of the swirl angle can not be separated from the influence of turbulence, which is however not sorted out until the next paragraph. The whole diffuser performance is analysed using the c_p (swirl angle; diffuser length) charts (for Mach number 0.1 is shown in Fig. 4) and the c_p (swirl angle, mass flow) chart (Fig. 5). These results are obtained for Mach numbers of 0.08…0.14 and Reynolds numbers of 31,700…35,500. The Mach number is calculated at the 50% channel height. The characteristic length in the Reynolds number is the length of the cross-section of the blade at the same height. The flow is assumed to be incompressible due to the relatively low Mach numbers.

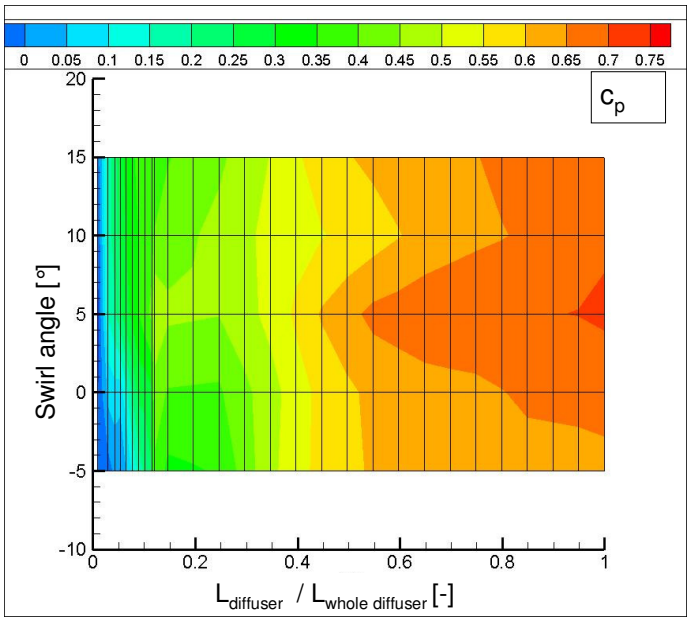

Figure 4: C_p in the whole diffuser as a function of length and the flow swirl angle at the inlet, Mach number 0.1

In Fig. 4 the pressure recovery is given as a function of the dimensionless length of the whole diffuser and the swirl angle in the inlet flow for the Mach number of 0.1. The best performance is achieved for the 5° positive swirl. Compared to

the other operating points, the highest c_p is registered for the whole diffuser for these conditions and the rise of c_p with increasing length is faster. With increasing swirl angle up to 10° and 15°, c_p is reducing slowly. Decreasing the swirl to -5° reduces c_p.

The performance of the diffuser is good for almost all of the studied mass flow and swirl values, with the pressure recovery not dropping below 0.55 for the most operating points. The trend observed for the different Mach numbers is shown in Fig. 6. Pressure recovery increases for positive swirl up to 5° and decreases for negative swirl up to -10°, compared to the operating points without swirl. A higher Mach number generally results in a higher c_p, but the trend swirl-c_p is constant. With growing Mach number, an increase in c_p is observed. The conditions with Mach number 0.08, 0.1, 0.12 and 0.14 lead to very similar correlations.

The pressure recovery for the Mach number of 0.08 is a little higher than for 0.1 for the swirl angle of -5° and 0°. The higher the Mach number, the steeper the swirl- c_p trend is. The Mach number of 0.12 gives the most favourable distribution in the range -5°…10°, but for the swirl of -10° the drop is significant.

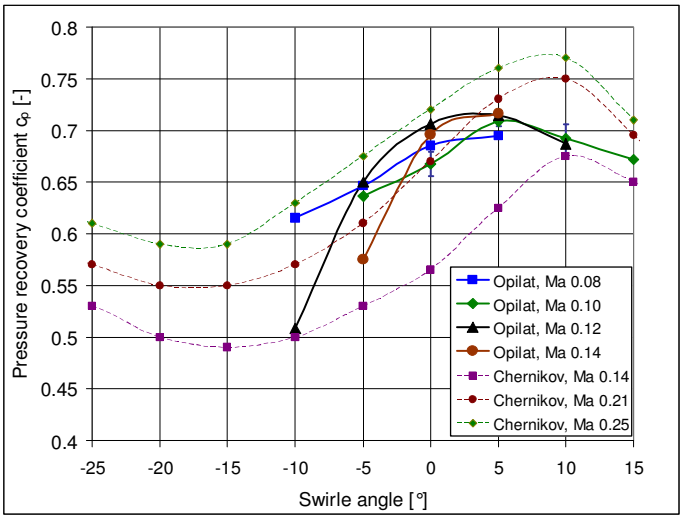

Figure 5: Pressure recovery for the whole diffuser as a function of swirl angle and Mach number

These results are interesting to compare with the results of Chernikov [10] as they show the same trend for c_p but for tests with incompressible flow. Chernikov's study of diffuser aerodynamic characteristics was performed on a similar diffuser but with a scaled turbine stage model and for Mach number in the diffuser inlet between 0.14 and 0.318. These results are shown in the diagram in Fig. 5. The difference in experimental values of c_p for the two test rigs is primarily due to the different geometric parameters (see Annex). Fig. 12 shows the ideal pressure recovery distribution for both test rigs explaining the difference in the results.

The increase of c_p for negative swirl angles higher than -15° found by Chernikov is not detected in the current research. For two tests at a Mach number of 0.1 and a swirl angle -10° and -15°, a certain rise of c_p was found but is not covered in this paper.

According to the performance charts of Sovran and Klomp' [5] for a diffuser with 15° annular and 5° conical parts, but with no turbine secondary flows, the flow separation would appear due to the aggressive opening angle. Stabilization of the boundary layer leads back to the effects introduced by the turbine rotor simulator.

The velocity distribution in the outlet of the annular diffuser in Fig. 6 helps to understand the processes in the diffuser. The uncertainty of the probe measurements is below 0.5% and thus is too little to be shown in Fig. 6. The casing and the hub boundary layer grow significantly within the annular diffuser. For the operating points with small negative swirl and without swirl, i.e. straight inflow, a back flow zone is observed at the shroud. For the operating point V102 with the lowest c_p of 0.63, the largest back flow zone is found. The small positive swirl smoothes the velocity profile near the shroud and prevents separation despite the aggressive opening angle of the diffuser (15°). In this case, the flow in the middle is decelerated due to the velocity decrease in the zone near the shroud. From previous studies [7] it is known that a strong swirl (without turbulence) causes separation on the hub, affecting the diffuser function; this tendency is suppressed due to the turbulent effects introduced by the operating bladed wheel. For the conditions with positive swirl, the turbulent energy in the flow is enough to prevent separation. For the operating point with 10° positive swirl the flow is decelerated at the shroud. The boundary layer is unstable but the separation tendencies are suppressed in this case what is also confirmed observing the filaments at the inner casing surface.

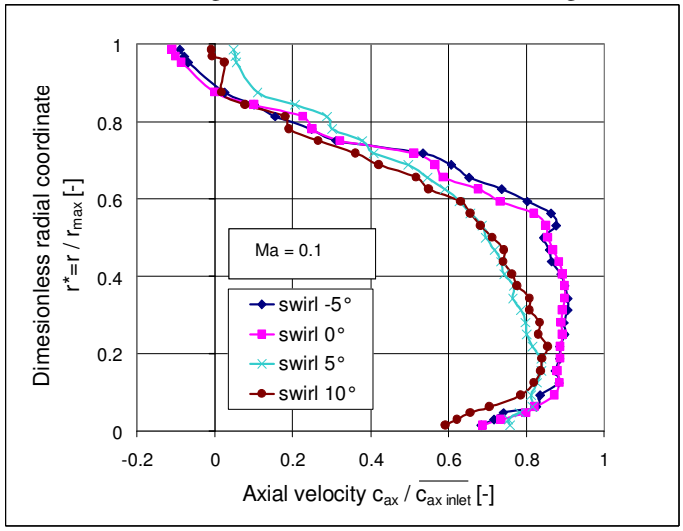

Figure 6: Velocity at the ring diffuser outlet as a function of swirl angle

INFLUENCE OF THE TURBULENCE INTENSITY ON THE PERFORMANCE OF THE DIFFUSER

Measurements with the PIV show the velocity distributions in the inlet of the diffuser. For the estimation of turbulence levels, rms velocities are used. 100 double-images are used to calculate velocities for each operating point. The position of the measurement section is shown in Fig. 8.

Velocity deviations (rms velocities) are found by averaging the PIV data by time. Because the measurement area is relatively small and is located right in the middle of the channel, the velocity is assumed constant for some height. Therefore, averaging is also performed by the height of the measurement region (from -5 mm to 10 mm) taking 15 points with 1 mm steps between them. The height here is not the radius of the diffuser but the vertical dimension in the plane perpendicular to the radius at the midspan. For the normalized turbulence intensity definition, the main velocity at the midspan is used. The correlations in Fig. 7 show the turbulent intensity in the flow entering the annular diffuser. This diagram shows high turbulence in the front part of the diffuser and a significant decrease with increasing length.

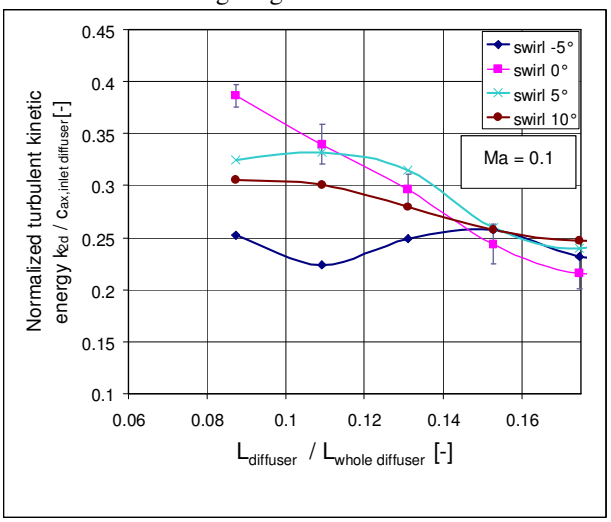

Figure 7: The turbulence intensity as a function of swirl, at the inlet of the annular diffuser

Turbulence caused by the rotating bladed wheel depends on the test conditions. The turbulence intensity is the highest for the conditions with a swirl angle of 0° and 5°, where the highest c_p of 0.7 is calculated. The turbulence intensity for conditions with a swirl angle of -5° is the lowest and c_p at 0.64 is also the lowest at this point. From the dimensionless length 0.18, the turbulence intensity does not depend on the entry conditions, due to mixing. The increase in turbulent intensity results in an increase in the pressure recovery. The curve for 15° is not presented because the PIV particle supply for this operating point was insufficient, and not enough images with sufficient particle density could be taken for averaging.

INFLUENCE OF THE BLADE WAKES ON THE PERFORMANCE OF DIFFUSER

In the analysis in the previous chapter, the averaged flow parameter took into account the turbulence introduced by the static entry grid and by the operation of the bladed wheel. In this chapter the analysis of velocity and vorticity is performed in order to learn about the origin of the unsteady effects. Fig. 8 displays the region where PIV measurements were taken with an evaluated data file to show the position of measurement.

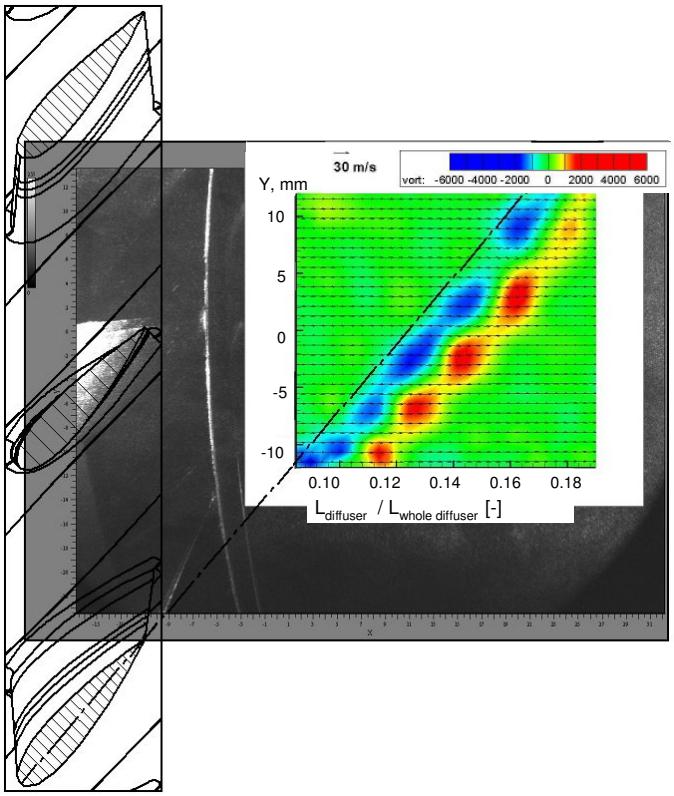

Figure 8: The vortex street behind the blade, Ma = 0.1

Vortex shedding is visualized by PIV in the diffuser inlet flow for the operating points V102-V106 and studied in order to estimate its influence on the performance of the diffuser. In this experiment, the rotating bladed wheel is driven by an electric motor to model the turbine part load conditions. In the flow behind the wheel the unsteady vortex structures detach from the trailing edges of the blades and form wakes. These structures are taken downstream by the main flow. Fig. 8 shows the vortex street in terms of vorticity behind the bladed wheel for the conditions with 10° positive swirl. A sketch of the bladed wheel is put on the picture with a dash-dotted blade center line. No dependence of the frequency with which the vortices separate from the blades on the c_p was observed. Assuming the Strouhal number being constant at 0.2 due to high Reynolds numbers, this frequency would not be expected to change, as is observed. This frequency also does not change

significantly with the changing swirl angle because of the main velocity being nearly constant in the inlet of the diffuser.

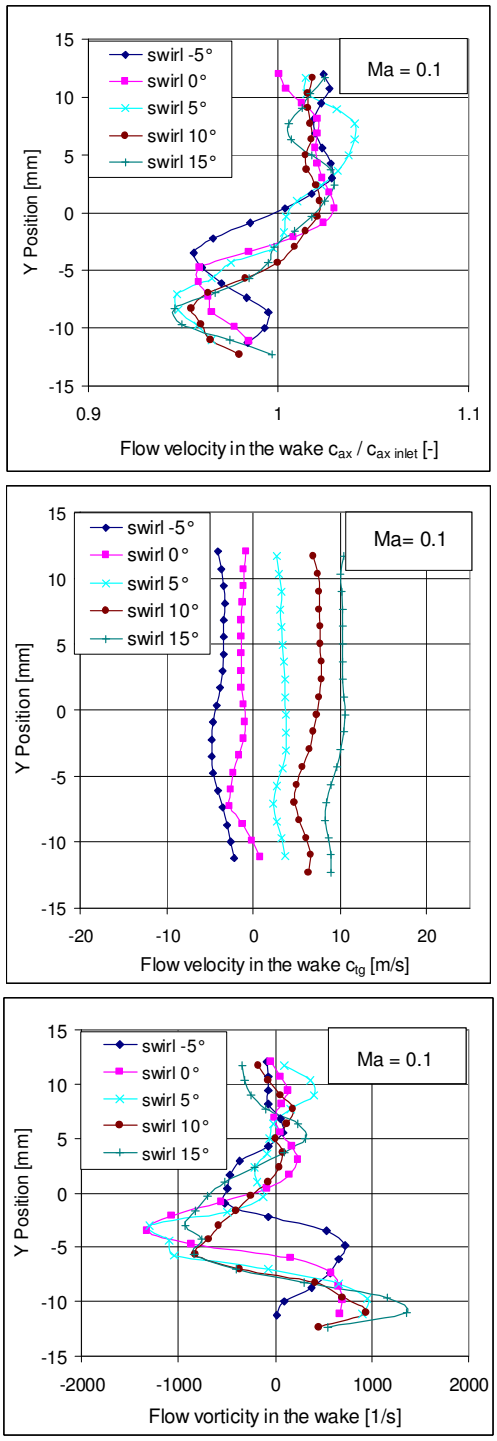

Figure 9: Blade wake at the annular diffuser inlet in terms of velocity and vorticity

The difference in the velocity and vorticity amplitude between the operating points can help to understand the impact of turbulence. In Fig. 9 the PIV data are shown, which were extracted from the velocity field at the diffuser length of 0.12. In the PIV measurement campaign, the diffuser operating points are studied taking batches of 100 double-images similar to those shown in Fig. 8. The pictures are sorted according to the angular position of the rotor. Those pictures for which the chosen blade is in the same position with an error of ± 0.5 mm are averaged and then evaluated in terms of velocity and vorticity. In the wake the velocity is lower than the main flow velocity. For the axial velocity, this reduction rises up to 4 m/s, which is about 10% of the main velocity in the test (Fig. 9). For the flows with positive swirl, the drop is shifted in the direction of swirl and is stronger. This can cause a rise in turbulence intensity resulting in higher pressure recovery. The vorticity amplitude is found to be the lowest for the operating point with the -5° swirl, correlating with the lowest pressure recovery for this point.

INFLUENCE OF THE TIP LEAKAGE FLOW ON THE PERFORMANCE OF THE DIFFUSER

In the correlations in Fig.10 the influence of leakage flow can be noticed for the most conditions, explaining the high c_p. The c_p trends for operating points with swirled tip leakage flow are given in Fig. 11. The flow does not separate for all operating points. The leakage flow is more developed in the velocity profile for conditions with positive swirl in the main flow. The combination of swirl in the main and the leakage flow affects the pressure recovery. The 10 to 15% rise of c_p is due to the leakage flow energising the boundary layer at the shroud and preventing separation.

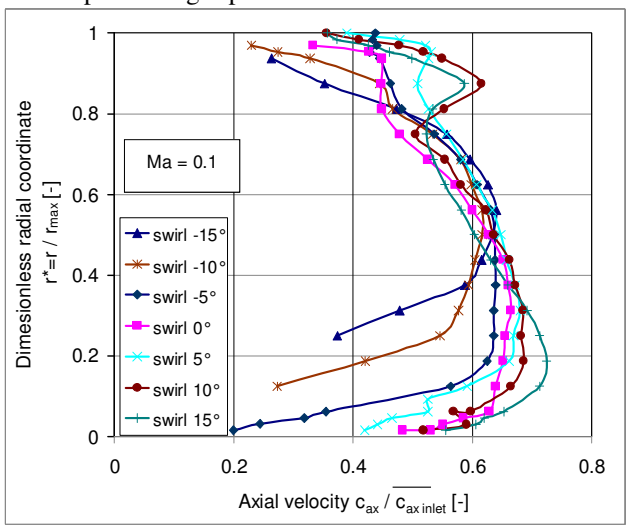

Figure 10: Velocity at the annular diffuser outlet as a function of swirl, Mach number 0.1, swirled leakage flow

Compared to the reference measurements of Chernikov, c_p is approximately 14% higher for all operating points except for one. This is due to the geometry differences between the test rigs. The trend is nevertheless similar at higher c_p for conditions with positive swirl, especially for the Mach number 0.12.

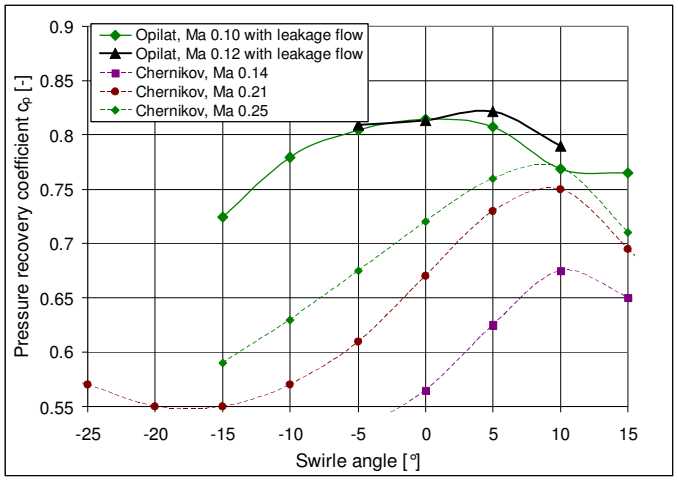

Figure 11: Pressure recovery for the whole diffuser as a function of swirl, with swirled leakage flow

CONCLUSIONS

Diffuser performance is explained based upon measurements of the phenomena in the diffuser flow. The influence of several main factors on pressure recovery, e.g. the swirl, the turbulence, the tip leakage flow, and the blade wakes is studied. It is demonstrated that the endoscopic PIV can be used for measurements on rotating machines.

Exhaust diffusers can be designed shorter and with improved performance by delaying the flow separation at the shroud. The pressure recovery coefficient c_p can be increased due to the unsteady flow conditions caused by the turbine.

The diffuser performance diagrams for the different inlet flow conditions introduced by the rotating bladed wheel show that positive swirl of about 5-10° has a positive effect on the pressure recovery while negative swirl, for the most cases, decreases c_p. This trend remains for all values of mass flow for the same diffuser geometry, but c_p increases with increased Mach number.

With the PIV, blade wakes and swirl are studied behind the rotating wake generator. Analysis of the PIV data shows that there is no direct dependence between c_p and the vortex shedding frequency. The rise of turbulence intensity in the inlet flow increases c_p, however. The performance diagrams are found to be similar to the correlations, obtained for a more gas turbine-like test rig with a scaled last turbine stage model and a similar geometry, thus verifying the test rig results.

For the operating points measured with a bladed wheel and additional leakage flow, pressure recovery is found to be very high. For this case, the correlations for different Mach numbers still show a dependence on the swirl angle, with the best performance for a small positive swirl.

ACKNOWLEDGMENTS

The authors greatly acknowledge the financial support of the Siemens/DAAD stipend program and the help of the staff of the Institute of Turbomachinery and Fluid Dynamics – TFD. Special thanks to Prof. V. Chernikov (Technical University of St. Petersburg) and Dr. Thomas Hammer (Siemens AG).

REFERENCES

[1] Lechner, C., Seume, J. (eds.), 2010. “Stationäre Gasturbinen”, 2nd ed., Berlin: Springer

[2] Fischer, W. J., 2010. “Siemens H class turbine, the SGT5-8000H ready for the market: a ‘giant’ gas turbine sets new benchmarks”, Mechanical Engineering-CIME, www.allbusiness.com/energy-utilities/utilities-industry-electric-power

[3] Balevic, D., Hartman, S., Youmans, R., 2009. “Heavy-Duty Gas Turbine operating and Maintenance considerations”, GER 3620L (11/09) GE Energy Atlanta, GA, www.gepower.com

[4] Kruse, H., Quest, J., 1982. “Experimentelle Untersuchungen an Nabendiffusoren hinter Turbinen”, MTZ-Motortechnische Zeitschrift, 44, pp. 13-17

[5] Sovran, G., Klomp, E. D., 1967. “Experimentally Determined Optimum Geometries for Rectilinear Diffusers with Rectangular, Conical or Annular Cross-Section”, Fluid Mech. Of Int. Flow, Symp., pp. 270-319

[6] Kluß, D., Stoff, H., Wiedermann, A., October 2009. “Effect of Wakes and Secondary Flow on Re-attachment of Turbine Exit Annular Diffuser Flow”, J. of Turbomachinery, Vol. 131 / 041012-3

[7] Fleige, H.-U., Riess, W., Seume, J.R., 2002. “Swirl and tip leakage flow interaction with struts in axial diffusers”, GT-2002-30491, ASME TURBO EXPO 2002, June 3-6, Amsterdam, The Netherlands

[8] Sieker, O., Seume, J.R., 2008. “Effects of Rotating Blade Wakes on Separation and Pressure Recovery in Turbine Exhaust Diffusers”, ASME TURBO EXPO 2008, June 9-13, Berlin, Germany

[9] Chernikov, V. A., 2008. “A Test Bench for Gas-dynamic Investigations of Exhaust Diffusers and Hoods of Turbines”, Thermal Engineering, Vol. 55, No. 6, pp. 499–505.

[10] Chernikov, V., Semakina, E., 2009. “Aerodynamic characteristics of the exhaust axial diffuser of the stationary gas turbine at various regimes of its operation”, No. 2 Journal “Energeticheskie machini i ustanovki”, Russian text

[11] Alhaj, O., Seume, J.R., 2010. “Optical Investigation of Profile Losses in a Linear Turbine Cascade”, GT2010-23166, ASME TURBO EXPO 2010, June 14-18, Glasgow, UK

[12] Woisetschläger, J., Mayrhofer, N., Hampel, B., Lang, H., Sanz W., 2003. “Laser-optical investigation of turbine wake flow”, Experiments in Fluids, Volume 34, No. 3, pp. 371-378

[13] Woisetschläger, J., Göttlich, E., 2008. “Recent Applications of Particle Image Velocimetry to Flow Research in Thermal Turbomachinery”, in: A. Schröder, C.M. Willert (eds.): Particle Image Velocimetry New Developments and Recent Applications, Topics of Applied Physics, Springer, Wien

[14] PIVVIEW2C/3C, Version 3.0, 2010. User Manual, PIVTEC, http://www.pivtec.com

ANNEX

GEOMETRIC PARAMETERS OF THE DIFFUSERS

Table 2: Geometric parameter of the TFD diffuser test rig

Diffuser	Area ratio AR [-]	Dimensionless length L_{ann}^{*} ; L_{con}^{*} [-]	ν [-]	Opening angle Θ_a [°]
15° annular diffuser	1.93	2.42	0.59	15
Conical diffuser	2.25/2.88	10.8/5.8	-	5
Diffuser	5.54	-	-	-

Table 3: Geometric parameter of the diffuser test rig of Chernikov

Diffuser	Area ratio AR [-] ("no hub")	Area ratio AR [-] ("with hub")	Dimensionless length L_{ann}^{*} ; L_{con}^{*} [-] ("no hub")	Dimensionless length L_{ann}^{*} ; L_{con}^{*} [-] ("with hub")	ν [-]	Opening angle Θ_a [°]
15° annular diffuser	1.43	1.61	2.38	-	0.55	10.26
Conical diffuser	2.4	3.05	12.03	6.51	-	4.8
Diffuser	4.9	-	-	-	-	-

Table 4: Geometric parameter of the diffuser test rig of Chernikov considering its modular design

Diffuser	Area ratio AR [-]	Dimensionless length L_{ann}^{*} ; L_{con}^{*} [-]	ν [-]	Half cone angle Θ_a [°]
15° annular diffuser (front part)	1.41	1.25	0.55	13.4
15° annular diffuser (rear part)	1.14	0.87	0.48	6.62

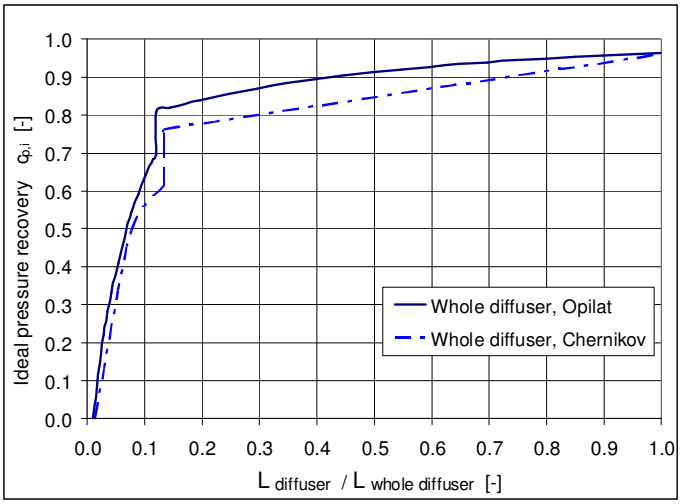

Figure 12: Ideal c_p whole diffuser

"With hub" means that the annular diffuser's outlet area is used for calculation of the parameter; "no hub" means that the conical diffuser's inlet area is used.